Zoledronate reduces microdamage accumulation in cortical bone of ovariectomized rats

Bohao Ning[1,2], Irène Londono[2], Catherine Laporte[2,3], Isabelle Villemure[1,2]*

[1] Department of Mechanical Engineering, Polytechnique Montréal, P.O. Box 6079, Station Centre-Ville, Montréal, QC H3C 3A7, Canada

[2] CHU Sainte-Justine Research Centre, 3175 Côte-Sainte-Catherine Road, Montréal, QC H3T 1C5, Canada

[3] Department of Electrical Engineering, École de technologie supérieure, 1100 Notre-Dame Street West, Montréal, QC H3C 1K3, Canada

* Corresponding author

Email: isabelle.villemure@polymtl.ca

Abstract

As a daily physiological mechanism in bone, microdamage accumulation dissipates energy and helps to prevent fractures. However, excessive damage accumulation might bring adverse effects to bone mechanical properties, which is especially problematic among the osteoporotic patients treated by bisphosphonates. Some pre-clinical studies in the literature applied forelimb loading models to produce well-controlled microdamage in cortical bone. Ovariectomized animals were also extensively studied to assimilate human osteopenic conditions. In the present study, we combined both experimental models to investigate microdamage accumulation in the context of osteoporosis and zoledronate treatment. Three-month-old normal and ovariectomized rats treated by saline or zoledronate underwent controlled loading on their right forelimb to create *in vivo* microdamage, which was then quantified by contrast-enhanced micro-CT imaging. Weekly *in vivo* micro-CT scans were taken to evaluate bone remodeling and to capture microstructural changes over time. After sacrifice, three-point-bending tests were performed to assess bone mechanical properties. Results show that the zoledronate treatment can reduce microdamage accumulation and improve the osteopenic conditions in cortical bone of ovariectomized rats. The balance between the damage repair and propagation might be dependent on the initial amount of damage. Moreover, the periosteal bone formation is correlated with the microdamage level, and the extent of which differs between normal, ovariectomized and zoledronate-treated animals. This study provides insights to the clinical optimization of osteoporosis treatment using bisphosphonates. The same experimental concept can be applied in future studies on microdamage and drug testing.

Keywords

Microdamage, remodeling, osteoporosis, zoledronate, micro-CT

1 Introduction

Bone microscopic damage (microdamage) accumulation is a physiological process that takes place during our daily activities [1, 2]. A balanced state of microdamage accumulation and repair can help to dissipate energy and to prevent fragility fractures [3, 4]. However, excessive levels of microdamage might lead to impaired bone mechanical properties [5-7]. Past studies in the literature have investigated how microdamage is initiated [8-11], accumulated [12-14], propagated [15-17], and repaired [18-21]. Pre-clinical studies applying mechanical loading on long bones of small laboratory animals showed the advantage of creating consistent damage levels that can be quantified by histology [19, 22, 23] or micro-CT-based methods [24-26].

Some experimental studies on microdamage made links to the condition of osteoporosis [10, 27, 28], a key factor that influences damage accumulation. Osteoporosis is a pathology characterized by low bone mineral density (BMD) [29, 30], which is especially common among the post-menopausal female population due to estrogen deficiency [31, 32]. Ovariectomized rodent models were widely used in pre-clinical studies due to their strong resemblance to the human osteoporotic conditions [33-36]. As one of the common treatments to osteoporosis, various types of bisphosphonates (BPs) were tested regarding their effects on bone quality improvement [37-41]. Zoledronate (zoledronic acid) is considered among the most potent BPs by inhibiting the bone resorption thus increasing the BMD [37, 42, 43].

However, the BP-reduced bone resorption can decrease the efficiency of microdamage repair [44-47], leading to increased damage density [48-50] and therefore impaired bone quality [41, 51, 52]. Clinical studies revealed that long term treatment of BPs can be associated with increased risk of atypical femoral fractures [53-56], atypical forearm fractures [57-60], and osteonecrosis of the jaw [61-63]. Although numerous translational studies were carried out to better understand these side effects [37, 44, 64, 65], the data are still lacking in terms of the direct relationships between microdamage accumulation, remodeling, and mechanical properties in the context of BP treatment. To fill in this knowledge gap, animal models are especially appropriate as they provide well-controlled experimental conditions.

In the present study, we combined the widely used ulna microdamage model with the well-established ovariectomized rat model to study microdamage accumulation in cortical bone. Our

objectives were: (1) to create and quantify *in vivo* microdamage in cortical bone of ovariectomized rats further treated by saline or zoledronate; (2) to quantify cortical bone remodeling and mechanical properties; (3) to evaluate the correlations between bone microdamage and remodeling or mechanical parameters.

2 Methods

2.1 Experimental design

Three months old female virgin CD IGS rats (n=48) were received from the Charles River Laboratories and were assigned to one of the following treatment groups: NOM (n=16), OVX (n=16) and ZOL (n=16). The NOM rats did not receive any surgery, while the OVX and ZOL rats received bilateral ovariectomy at the animal supplier on week 0 (Fig. 1). All rats arrived at the animal facility of the Sainte-Justine University Hospital Center on week 1 and were housed in cages of two with free access to food and water. They lived a light/dark circle of 12 hours at about 23°C and 21% humidity. One week of acclimation was allocated before the start of the experiment on week 2. The Institutional Committee for Good Animal Practices in Research of the Sainte-Justine University Hospital Center approved the animal experiments in this study.

As shown in Fig. 1, the rats received *in vivo* micro-CT scans on weeks 2, 9, 10, 11 and 12 to follow up on the microstructural changes in their forelimbs and hindlimbs (section 2.2). They also received subcutaneous injections on weeks 2, 6 and 10, where the NOM and OVX rats were given sterile saline (1 mL/kg) and the ZOL rats were given zoledronate (100 µg/kg). The dose of the zoledronate was based on past rodent models to reflect the clinical dose used for osteoporosis treatment in humans [38, 42, 66]. On week 10, all rats received a single session of mechanical loading (section 2.3) on their right forelimb to generate microdamage *in vivo*. Half of the rats (8 from each group) were sacrificed 5 days post-loading and the other half 15 days post-loading to quantify the amount of microdamage using contrast-enhanced micro-CT imaging (section 2.4). After sacrifice, all the forelimb samples received a three-point-bending test to evaluate their mechanical properties (section 2.5).

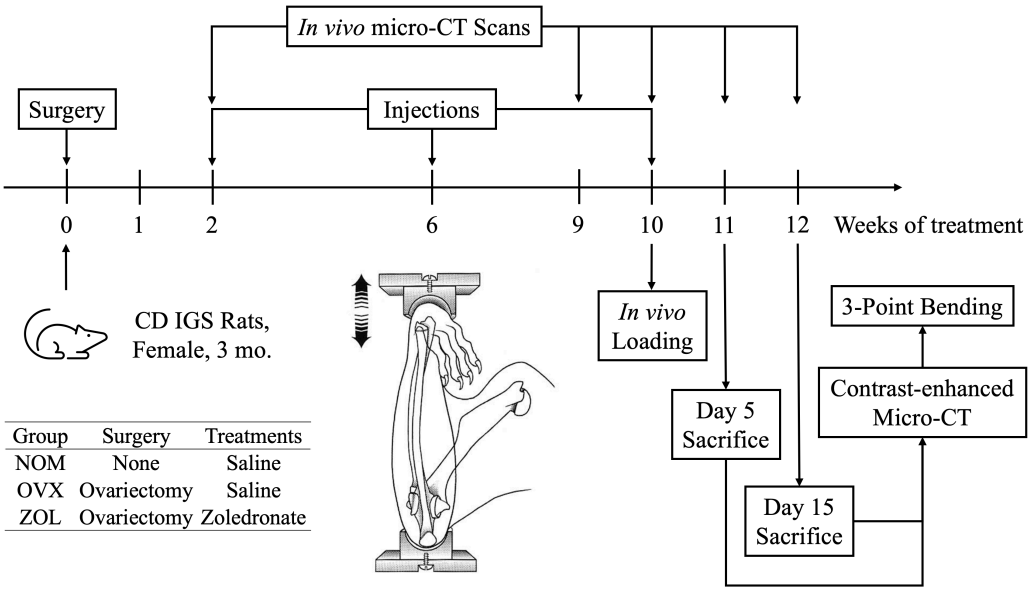

Fig. 1. Experimental design. The forelimb loading diagram was adapted from [67] with permission obtained from the publisher.

2.2 *In vivo* micro-CT imaging

On week 2, *in vivo* micro-CT scans were acquired using a SkyScan 1176 microtomograph (Bruker microCT N.V., Kontich, Belgium) on rats' right forelimb and right hindlimb to capture the initial bone microstructure (Fig. 1). On weeks 9, 10, 11 and 12, additional weekly scans were performed on both forelimbs to calculate the remodeling rates. The right hindlimbs were scanned on week 12 to confirm the effects of ovariectomy and zoledronate treatment. Rod-shaped phantoms of 0.25 and 0.75 g/cm^3 were scanned every day for calibration purposes. All the scans were performed at an image resolution of 8.74 µm, using a filter of 1 mm Al, exposure time of 1200 ms, voltage of 65 kVp, current of 300 µA, rotation angle of 0.5° / 180°. The rats were under isoflurane anesthesia (2.5%) supplied by oxygen (1.5 L/min) during the scans, which lasted about 11 minutes each. The radiation exposure was estimated to be about 1.08 Gy for each scan, calculated by the CTion software (Bruker microCT N.V., Kontich, Belgium) [68].

After the scans, the images were reconstructed using the NRecon software (Bruker microCT N.V., Kontich, Belgium). The dynamic range was set to [0, 0.06] (attenuation coefficient) and the post-alignment was adjusted visually starting from a default value proposed by the software. Beam-hardening correction was applied at 20% and ring-artifact correction was set to 5. For the subsequent image analysis, volumes of interest (VOIs) were extracted using CT Analyzer (Bruker

microCT N.V., Kontich, Belgium). The ulna and radius VOIs were centered at mid-third diaphysis, expanding for about 20% of total bone length. This location was shown to receive the most flexion in response to axial forelimb compression [23, 24]. The proximal tibia VOIs of 2 mm long were taken starting from 2 mm distal to the proximal growth plate. The trabecular VOIs were then segmented using a semi-automatic selection tool in CT Analyzer.

To calculate the weekly remodeling parameters between weeks 9 and 12, the images of ulna and radius from weeks 10, 11 and 12 were rigidly registered to the baseline scans of week 9 using custom software developed using ITK (Kitware Inc., Clifton Park, NY, USA) [69]. Automatic registration was based on a regular step gradient optimizer with mutual information as the optimization metric. Once the images were registered, a previously validated MATLAB-based program was used to calculate the remodeling parameters on the periosteum of ulna and radius [70], with empirically adjusted segmentation parameters. The following remodeling parameters were analyzed in terms of volume, surface, and thickness: newly mineralized bone volume per bone volume (MV/BV), newly eroded bone volume per bone volume (EV/BV), newly mineralized bone surface per bone surface (MS/BS), newly eroded surface per bone surface (ES/BS), mineral apposition rate (MAR, μm/day), and mineral resorption rate (MRR, μm/day).

The dynamic histomorphometry was performed using CT Analyzer [71, 72]. The following cortical parameters were evaluated for radius and ulna: tissue mineral density (TMD, g/cm^3), cortical bone volume (Ct.BV, mm^3), average cross-sectional cortical area (Ct.Ar, mm^2), and average cortical thickness (Ct.Th, μm). The following trabecular parameters were evaluated for tibia: bone mineral density (BMD, g/cm^3), trabecular bone volume (Tb.BV, mm^3), trabecular bone surface area (Tb.BS, mm^2), trabecular bone volume fraction (Tb.BV/TV), trabecular thickness (Tb.Th, μm), trabecular number (Tb.N, 1/mm), trabecular separation (Tb.Sp, μm), and connectivity density (Conn.Dn, 1/mm^3).

2.3 *In vivo* mechanical loading

The *in vivo* loading session was applied on week 10 (Fig. 1). One hour before loading, the rats were given a dose of buprenorphine (0.05 mg/kg) subcutaneously as a sedative and an analgesic. Ten minutes before loading, the rats were put into anesthesia via isoflurane (3.0%) supplied by

oxygen (1.8 L/min). They were laid on their back, supported by a surface warming pad (36 to 37°C). The *in vivo* loading, performed using a Mach-1 micromechanical system (Biomomentum Inc., Laval, QC, Canada), started with a preconditioning session of 50 sinusoidal cycles of cyclic compression (amplitude of 1 mm, frequency of 2 Hz).

The subsequent main loading step was based on sinusoidal cyclic compression as well, with a physiological frequency of 2 Hz and a peak force of 16 N. The loading was stopped when one of the following equivalent conditions was satisfied: the accumulated actuator displacement reached 0.60 mm, or 5040 cycles was completed. The dual stopping criteria served to prevent the forelimb from fracture, which corresponded to 58% of the fracture point (1.0391 mm of actuator displacement) based on our preliminary tests where 90% of the rats (n=20 in total) did not encounter a fracture within 0.60 mm of accumulated actuator displacement (equivalent to 5040 cycles). Right after the *in vivo* loading, the rats were given a dose of metacam (1 mg/kg) subcutaneously to relieve potential pain caused by loading. The rats were followed up 1h, 4h, 24h, 48h and 72h after the loading session for assessment of their well-being, based on which no additional analgesic was provided.

2.4 $BaSO_4$ Staining and contrast-enhanced micro-CT imaging

Once the rats were sacrificed by CO_2 asphyxiation and decapitation, the forelimbs were collected, removed of soft tissues, and dissected into individual ulna and radius samples. The samples were wrapped by phosphate-buffered-saline (PBS)-soaked gauze and stored in tubes of 5 mL in a freezer (-20°C). Five days after the dissection, the samples were thawed for barium sulfate ($BaSO_4$) contrast staining according to a previously validated method [24-26, 73-75]: the ulna and radius samples were immersed in equally mixed solution of 0.5 M barium chloride ($BaCl_2$), acetone, and PBS solution for 3 days under vacuum; followed by another 3 days of staining in equally mixed solution of 0.5 M sodium sulfate (Na_2SO_4), acetone, and PBS solution under vacuum. After the staining, the samples were gently washed and wrapped in PBS-soaked gauze for contrast-enhanced micro-CT imaging. The scans were performed using the SkyScan 1176 at an image resolution of 8.74 μm, using a filter of 1 mm Al, exposure time of 1500 ms, voltage of 65 kVp, current of 385 μA, rotation angle of 0.25° / 180°. After the scans, the samples were wrapped again in PBS-soaked gauze and put back into tubes for storage (-20°C). The micro-CT images were reconstructed using

the NRecon software. The dynamic range was set to [0, 0.12] (attenuation coefficient) and the post-alignment was adjusted visually starting from a default value proposed by the software. Beam-hardening correction was applied at 20% and ring-artifact correction was set to 5.

To evaluate the microdamage accumulated in radius and ulna, the same VOIs were used as explained in section 2.2. The microdamage was intended to be evaluated inside the original pre-loading bone volume. Therefore, the newly formed woven bone on the ulna samples was excluded by registering the ulna VOIs to the images of week 10 (pre-loading images). The image registration method was the same as explained in section 2.2. The registration step was not performed for the radius VOIs as their newly formed bone was not voluminous enough to affect the staining procedure based on visual verifications. Subsequently, the VOIs were imported into MATLAB R2018b (The MathWorks, Inc., Natick, MA, USA) for microdamage quantification. A customized script evaluated the stained volume over the total bone volume (SV/BV), which reflects the overall extent of microdamage based on methods developed in previous studies [24, 25]. The threshold applied was 0.67 g/cm^3 and 1.77 g/cm^3 for the bone volume and the stained volume respectively. These thresholds were determined based on histogram analysis for each of the 3D datasets. We verified that the threshold for the stained volume was well above the dynamic range of the bone mineral density. For each pair of bones, the difference in SV/BV between the loaded and the control samples was calculated to derive a new parameter ΔSV/BV, which reflects the overall microdamage quantity resulting from the applied *in vivo* loading, excluding the effects of daily damage and surface staining. Very few pairs of VOIs (3.5%) showed slightly higher SV/BV on the control sample than on the loaded sample. In this case, we took the value of ΔSV/BV to be 0 and interpreted as insignificant damage produced by the *in vivo* loading.

2.5 Three-point-bending

One week after the contrast-enhanced micro-CT, the ulna and radius samples were thawed to room temperature (about 23°C) for the three-point-bending procedure. The bending was performed using the Mach-1 micromechanical system and a customized bending platform. The span between the two sample supports was set to 18 mm. The ulna was loaded in the medio-lateral direction and the radius was loaded in the anterior-posterior direction (Fig. 2) to ensure stable positioning of the

samples. The actuator displacement speed was set to 0.01 mm/s and the data acquisition was performed at a frequency of 100 Hz.

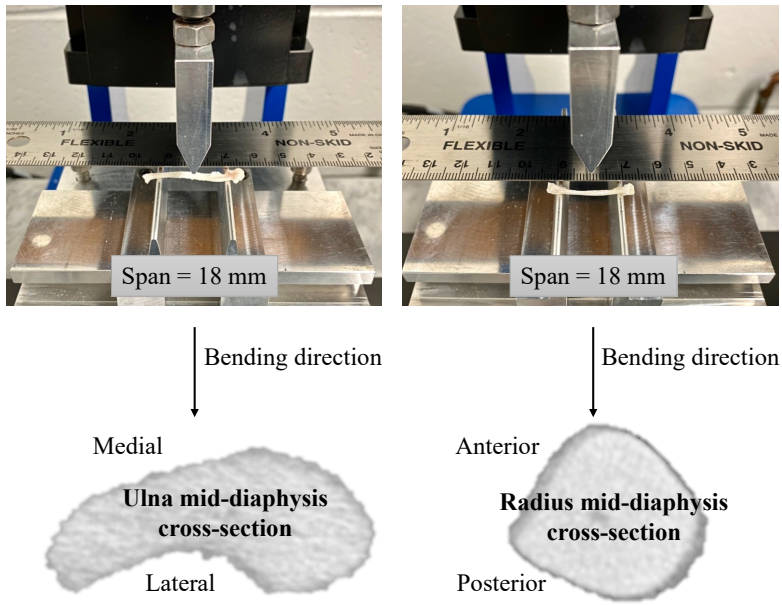

Fig. 2. Three-point-bending setup for the ulna and radius samples. Samples within the experimental setup are shown in the top row, and cross-sectional views are shown in the bottom row.

After the bending tests, the force-displacement curves were analyzed using the Mach-1 Analysis software (Biomomentum Inc., Laval, QC, Canada) to measure the following structural properties: ultimate force (F_u, N), yield force (F_y, N), stiffness (S, N/mm), pre-yield displacement (D_{pre}, mm), and pre-yield energy (U_{pre}, mJ). To estimate the material (tissue) properties using beam theory equations [50, 52, 76-78], the *ex vivo* micro-CT images of the samples were used to calculate the second moment of area, maximum diameter of the loaded section, and the distance from the neutral axis to the bone surface with the BoneJ plugin [79] of the FIJI software [80]. The following material properties were calculated: ultimate stress (σ_u, MPa), yield stress (σ_y, MPa), Young's modulus (E, GPa), pre-yield strain (ϵ_{pre}, $\mu\epsilon$) and pre-yield toughness (u_{pre}, MPa).

2.6 Statistics

The statistical tests were performed using SPSS Statistics v26 (IBM Corp, Armonk, NY, USA). Different ANOVA tests were performed for each parameter as shown in Table 1. The hypotheses of the ANOVA tests were verified when applicable. The boxplots revealed very few outliers (less

than 3.1%) which were not removed since they did not consist of data entry or measurement errors to our knowledge. The Shapiro-Wilk's test and Normal Q-Q Plots determined that the data were normally distributed in general. The Levene's test for equality of variances was performed, showing that variances were homogenous for the vast majority of the data groups. The ANOVA test was performed because it is somewhat robust to heterogeneity when the group sample sizes are equal, data are normal, and the ratio of the largest group variance to the smallest group variance is less than 3 [81-84]. The Box's test determined that the homogeneity of covariances was also met for most of the data groups. As determined by the Mauchly's test of sphericity, the assumption of sphericity was violated for some data groups. Thus, the Greenhouse–Geisser correction was applied when interpreting the within-subject effects. Bonferroni correction was applied for the *p*-value calculation in the *post hoc* tests and multiple comparisons, after which the statistical significance level (alpha) was set to 0.05. Additional data of interest are reported for the results of bone mechanical properties ($p < 0.10$).

Table 1. Summary of ANOVA tests performed. The treatment factor refers to the rat group NOM, OVX and ZOL. The recovery factor refers to the sacrifice time point of day 5 or day 15 post-loading. The bone side factor refers to left (control) or right (loaded) side. The time points vary from week 2 to week 12 of the experiment.

Parameter	ANOVA Type	Between-subjects Factors	Within-subjects Factor
Bone microdamage	Two-way	Treatment, recovery	n/a
Bone remodeling	Three-way mixed	Recovery, bone side	Time Points
Bone mechanical properties	Three-way	Treatment, recovery, bone side	n/a
Dynamic histomorphometry	Two-way mixed	Treatment	Time Points

Besides the ANOVA analyses, two-tailed t-tests were performed for the bone microdamage parameter ΔSV/BV and the bone mechanical properties to compare between the radius and ulna for each rat group. Another two-tailed t-test was performed for the dynamic histomorphometry parameters on week 12 to compare between left (control) and right (loaded) bone (radius or ulna) of the same rat. The statistical significance level (alpha) was set to 0.05 for all the t-tests. The two-tailed Spearman's rank-order correlation was used to evaluate the correlations between the bone microdamage parameter SV/BV and bone remodeling or mechanical properties. The analysis between SV/BV and the remodeling parameters was only performed for the rats which were sacrificed 15 days post-loading, since the remodeling parameters of the day 5 rats were not available. The assumption of a monotonic relationship between all the data pairs was verified using

scatterplots. For each analysis, Spearman's correlation coefficient is reported if there was statistical significance ($p < 0.05$). Additional data of interest ($p < 0.15$) are reported as well.

3 Results

3.1 Bone microdamage

Example visualizations of ulna microdamage are shown in Fig. 3, representative of each treatment group and the side of bone. The volume of formed, resorbed and constant bone were identified based on the registration results between the stained VOIs (week 12) and the pre-loading VOIs (week 10). The damage (stained) volume was identified based on the threshold analysis of the stained VOIs.

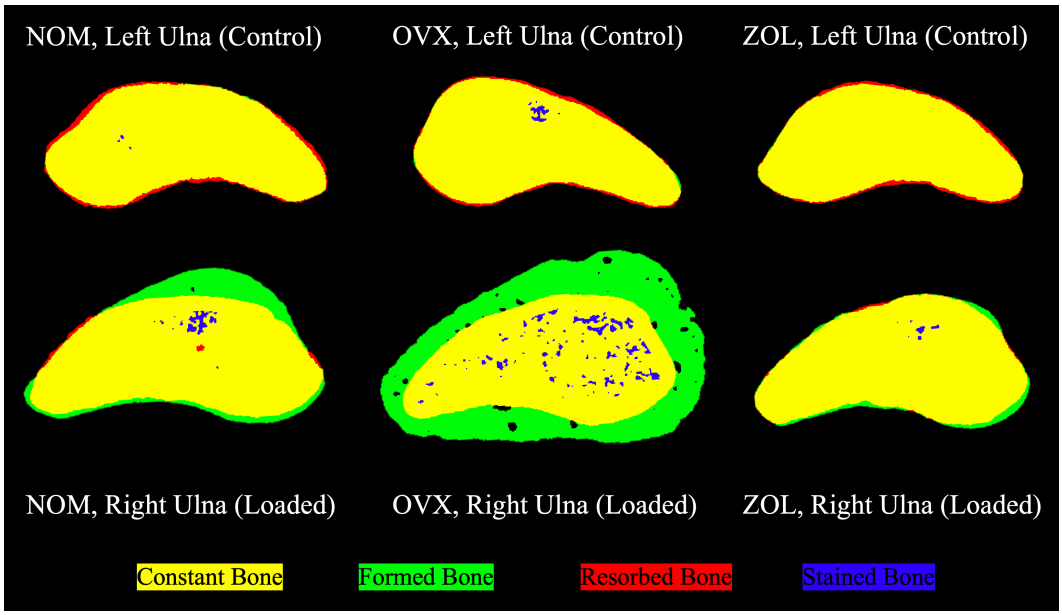

Fig. 3. Example visualization of the ulna microdamage results shown in binarized cross-sectional area. The top row shows the control ulnae of each group, and the bottom row shows the loaded ulnae. Based on the image registration results and threshold analysis, the constant, formed, resorbed, and stained bone volume are shown in yellow, green, red, and blue, respectively.

The results of ΔSV/BV are shown in Fig. 4. For the ulna, both NOM and OVX rats had increased values over time; the ZOL ulnae were at a lower level on day 15 compared to the OVX. As for the radius, the NOM rats had decreased values from day 5 to day 15; the ZOL rats showed relatively lower levels compared to the NOM rats on day 5 post-loading, and to the OVX rats on day 15.

Based on the t-test performed between ΔSV/BV of radius and ulna, the ulna showed more microdamage than the radius for all the three rat groups ($p < 0.01$).

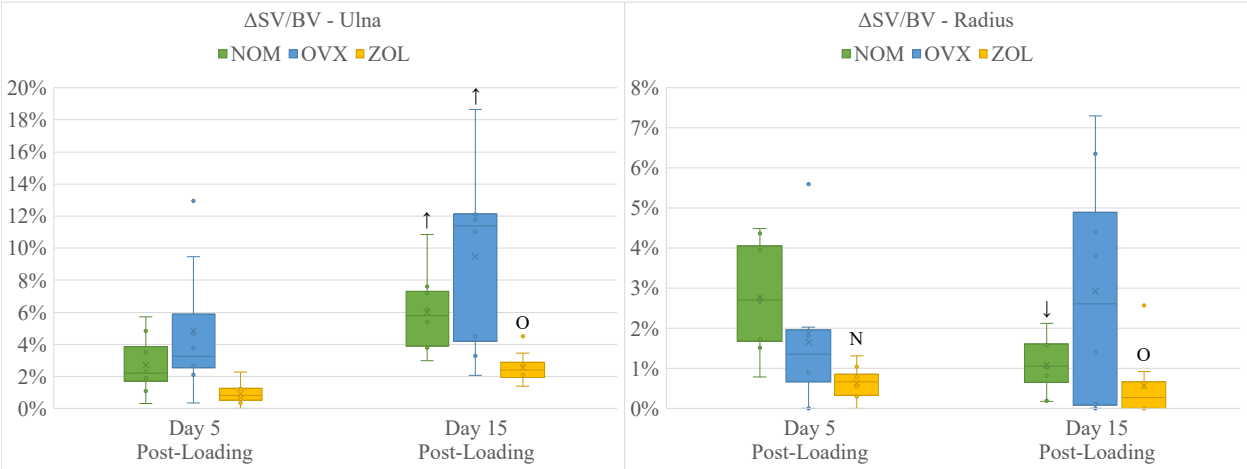

Fig. 4. ΔSV/BV for ulna and radius, reflecting the overall microdamage accumulated by *in vivo* loading. "↑" or "↓" refers to a significant increase or decrease compared to the previous time point. "N" or "O" refers to a significant difference compared to the NOM or OVX group. Bonferroni correction was used for *post hoc* tests and multiple comparison adjustments, after which the statistical significance level (alpha) was set to 0.05.

3.2 Bone remodeling

The results of remodeling are shown in Fig. 5 for ulna and in Supplementary Fig. 1 for radius. Since ulna and radius showed similar general tendencies, the following results are focused on ulna.

3.2.1 Effects of recovery time

MV/BV and MS/BS generally increased over time (↑). MAR declined in general (↓). EV/BV and ES/BS remained on a relatively constant level. MRR showed decreasing tendency (↓).

3.2.2 Effects of treatment groups

The OVX (control) and ZOL (control) showed lower MV/BV and MS/BS compared to the NOM (control) on week 11 and 12 (N). The ZOL (loaded) showed lower MV/BV and MS/BS compared to the NOM (loaded) and OVX (loaded) on week 11 and 12 (NO). The MV/BV and MS/BS showed approximatively three levels on week 12: the NOM (loaded) and OVX (loaded) on a higher level, the NOM (control) and ZOL (loaded) on the middle level, then the OVX (control) and ZOL (control) on a relatively lower level. The ZOL (loaded) had lower MAR than both NOM (loaded) and OVX (loaded) on week 12 (NO). The OVX (control) and ZOL (control) showing lower MRR

than the NOM (control) on week 11 and 12 (N). In general, the resorption parameters showed less between-group differences than their formation counterparts.

3.2.3 Effects of loading

Contralateral differences of each parameter were not always clear, and statistically significant results were mostly found on week 12 (*).

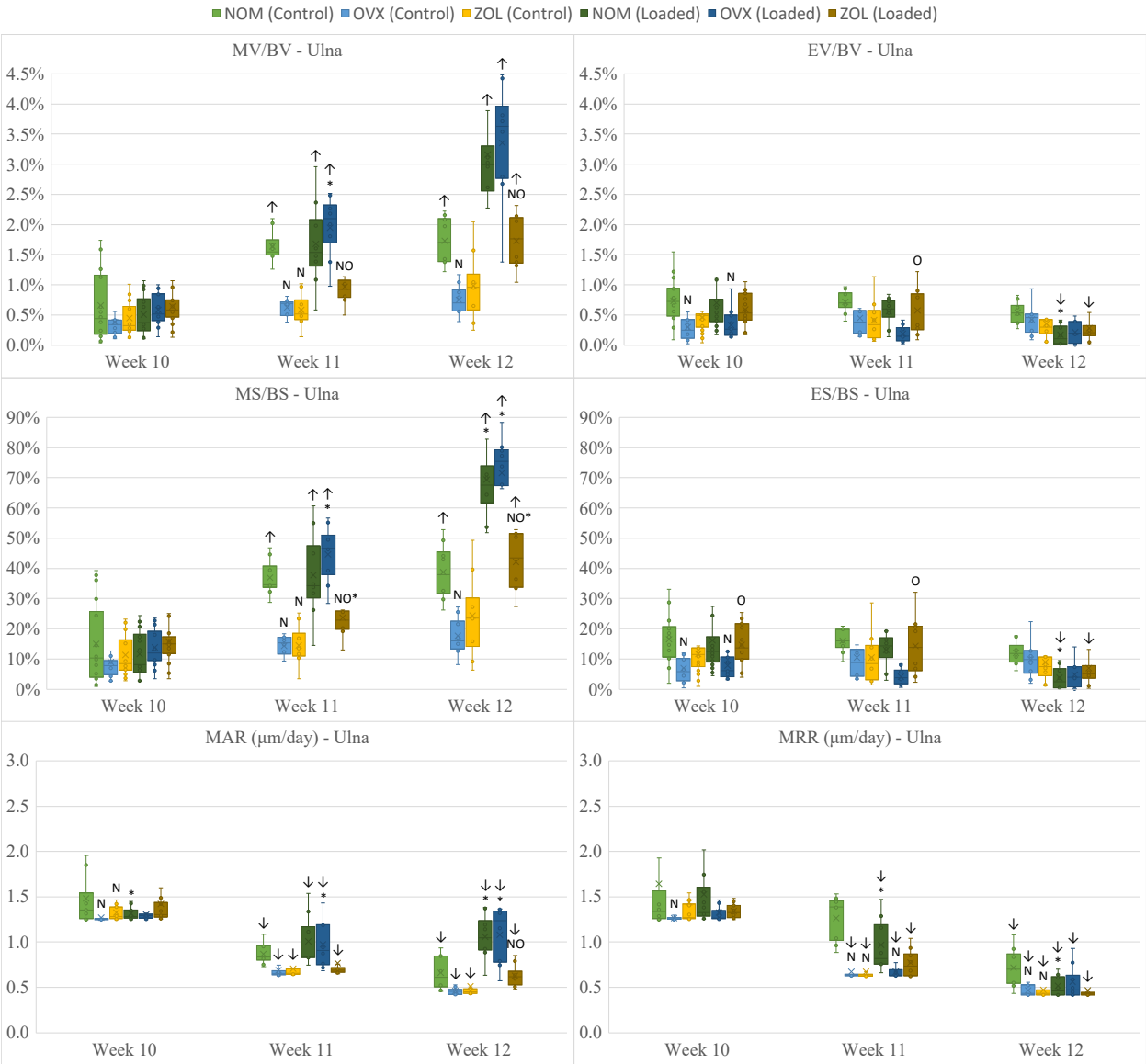

Fig. 5. Ulnar remodeling parameters shown in boxplots. "↑" or "↓" refers to a significant increase or decrease compared to week 10. "N" or "O" refers to a significant difference compared to the NOM or OVX group. "*" refers to a significant difference between the left and right ulna. Bonferroni correction was applied for the *p*-value calculation in the *post hoc* tests and multiple comparisons, after which the statistical significance level (alpha) was set to 0.05.

3.3 Bone mechanical properties

The results of the mechanical properties (structure and material) are shown in Table 2 for the ulna samples and in Supplementary Table 1 for the radius samples. Compared to ulna, radius had significantly ($p < 0.01$) stronger structural parameters except for U_{pre}. The differences between ulna and radius are less consistent for the material properties. In general, there were more data points of statistical significance in radius than in ulna.

Table 2. Ulnar mechanical properties tested by three-point-bending. The structural properties are shown on the top half of the chart, and their material counterparts are at the bottom half. "↑" or "↓" refers to a significant increase or decrease compared to day 5. "N" or "O" refers to a significant difference compared to the NOM or OVX group. "*" refers to a significant difference between the left (control) and right (loaded) ulna. Bonferroni correction was applied for the *p*-value calculation in the *post hoc* tests and multiple comparisons, after which the statistical significance level (alpha) was set to 0.05. The result of a *p*-value between 0.05 and 0.10 was marked in red. The cells of statistical significance are in bold.

Time	VOI	Group	F_u (N)		F_y (N)		S (N/mm)		D_{pre} (mm)		U_{pre} (mJ)	
Day 5	Control	NOM	11.68 ± 1.37		9.06 ± 0.87		17.54 ± 2.09		0.5957 ± 0.0636		2.67 ± 0.33	
		OVX	13.41 ± 1.86		10.34 ± 1.94		**26.23 ± 5.66**	N	0.5366 ± 0.0686		2.70 ± 0.72	
		ZOL	**16.42 ± 3.58**	NO	**11.47 ± 2.12**	N	**30.05 ± 13.55**	N	0.5542 ± 0.1359		3.10 ± 1.02	
	Loaded	NOM	11.94 ± 1.47		9.43 ± 1.23		17.70 ± 1.71		0.6159 ± 0.0559		2.87 ± 0.57	
		OVX	12.69 ± 2.32		10.26 ± 1.98		25.09 ± 8.33		0.5774 ± 0.1261		2.83 ± 0.68	
		ZOL	**16.63 ± 3.50**	NO	**11.84 ± 2.66**	N	**26.59 ± 7.16**	N	0.6056 ± 0.1025		3.43 ± 1.16	
Day 15	Control	NOM	12.93 ± 2.34		10.08 ± 1.62		22.33 ± 5.84		0.6437 ± 0.0886		2.87 ± 0.48	
		OVX	12.47 ± 1.38		9.37 ± 0.87		**20.20 ± 3.94**	↓	0.5852 ± 0.0894		2.63 ± 0.30	
		ZOL	**16.65 ± 2.22**	NO	**11.72 ± 1.68**	O	**31.39 ± 5.58**	NO	**0.5467 ± 0.0813**	N	2.99 ± 0.66	
	Loaded	NOM	**14.22 ± 1.61**	↑	10.39 ± 1.19		**24.38 ± 3.69**	↑	**0.5578 ± 0.0816**	*	2.88 ± 0.62	
		OVX	14.23 ± 2.22		9.87 ± 1.58		**26.47 ± 7.04**	*	**0.4741 ± 0.0448**	↓*	2.33 ± 0.44	
		ZOL	16.47 ± 2.11		**11.84 ± 1.72**	O	28.96 ± 4.80		0.5381 ± 0.0310		**3.14 ± 0.57**	O

Time	VOI	Group	σ_u (MPa)		σ_y (MPa)		E (GPa)		ϵ_{pre} (με)		u_{pre} (MPa)	
Day 5	Control	NOM	275.63 ± 14.58		214.29 ± 12.83		22.53 ± 2.10		10,998 ± 1,477		1.17 ± 0.15	
		OVX	262.79 ± 20.45		202.53 ± 28.18		25.42 ± 3.07		10,718 ± 1,034		1.06 ± 0.26	
		ZOL	290.13 ± 13.96		205.55 ± 26.36		24.67 ± 5.84		11,326 ± 2,368		1.16 ± 0.36	
	Loaded	NOM	262.81 ± 22.70		207.34 ± 15.50		20.23 ± 1.83		11,910 ± 1,291		1.21 ± 0.18	
		OVX	243.61 ± 28.97		196.84 ± 25.94		23.80 ± 6.39		11,620 ± 2,732		1.10 ± 0.27	
		ZOL	**288.54 ± 43.35**	O	205.64 ± 34.34		21.88 ± 3.86		12,648 ± 2,102		1.25 ± 0.37	
Day 15	Control	NOM	289.05 ± 22.83		214.10 ± 15.01		22.41 ± 2.32		**13,507 ± 928**	↑	**1.42 ± 0.18**	↑
		OVX	**250.86 ± 21.28**	N	**188.50 ± 12.61**	N	**21.12 ± 3.98**	↓	**11,287 ± 1,805**	N	**1.02 ± 0.14**	N
		ZOL	**283.42 ± 28.60**	O	199.72 ± 23.32		25.16 ± 3.72		**11,608 ± 1,876**	N	**1.08 ± 0.24**	N
	Loaded	NOM	274.10 ± 18.20		203.02 ± 15.16		21.31 ± 1.51		**13,618 ± 1,379**	↑	1.36 ± 0.20	
		OVX	253.65 ± 34.43		**176.50 ± 29.40**	N↓	22.63 ± 3.97		**9,820 ± 1,043**	N↓*	**0.87 ± 0.20**	N↓
		ZOL	268.66 ± 23.23		192.86 ± 16.92		**21.97 ± 2.52**	*	**11,551 ± 984**	N	**1.10 ± 0.17**	N

3.3.1 *Effects of recovery time*

From day 5 to day 15 post-loading: the NOM ulnae (control) showed increased ϵ_{pre} and u_{pre} (↑); the NOM ulnae (loaded) showed increased F_u, S and ϵ_{pre}(↑); the OVX ulnae (control) had decreased S and E (↓); the OVX ulnae (loaded) had decreased D_{pre}, σ_y, ϵ_{pre} and u_{pre} (↓). No significant effects of recovery time were found for the ZOL ulnae.

3.3.2 *Effects of treatment groups*

The ZOL ulnae showed higher F_u, F_y and S compared to the NOM or OVX ulnae (N or O) at most of the relevant data points. Their material counterparts σ_u, σ_y and E showed less consistent results. Both OVX and ZOL ulnae had lower ϵ_{pre} and u_{pre} than the NOM on day 15 (N). These differences were not clear for the structural parameters D_{pre} and U_{pre}.

3.3.3 *Effects of loading*

There were a few data points showing contralateral differences (control vs loaded), which were mostly found in results of loaded samples on day 15 (*).

3.4 Dynamic histomorphometry

The results of dynamic histomorphometry are shown in Table 3 for ulna, in Table 4 for tibia, and in Supplementary Table 2 for radius.

Table 3. Ulnar dynamic histomorphometry. "↑" refers to a significant increase compared to week 2. "N" or "O" refers to a significant difference compared to the NOM or OVX group. "*" refers to a significant difference between the left (control) and right (loaded) ulna. Bonferroni correction was applied for the *p*-value calculation in the *post hoc* tests and multiple comparisons, after which the statistical significance level (alpha) was set to 0.05. The cells of statistical significance are in bold.

Time	VOI	Group	TMD (g/cm^3)		Ct.BV (mm^3)		Ct.Ar (mm^2)		Ct.Th (μm)	
Week 2	Baseline	NOM	1.03 ± 0.03		10.04 ± 0.51		1.26 ± 0.07		157.85 ± 16.87	
		OVX	**0.97 ± 0.05**	**N**	10.44 ± 0.69		1.33 ± 0.08		**142.08 ± 22.36**	**N**
		ZOL	0.99 ± 0.02		10.23 ± 1.01		1.31 ± 0.11		**152.02 ± 10.48**	**N**
Week 12	Control	NOM	1.07 ± 0.05		**11.00 ± 0.80**	↑	**1.35 ± 0.09**	↑	**241.60 ± 9.81**	↑
		OVX	**1.08 ± 0.03**	↑	**12.03 ± 0.93**	↑	**1.43 ± 0.11**	↑	**177.92 ± 8.97**	**N↑**
		ZOL	**1.06 ± 0.06**	↑	**13.01 ± 1.00**	**N↑**	**1.58 ± 0.10**	**NO↑**	**170.34 ± 26.30**	**N**
	Loaded	NOM	1.04 ± 0.05		**12.22 ± 1.16**	↑*	**1.50 ± 0.16**	↑*	**255.91 ± 9.02**	↑*
		OVX	**1.02 ± 0.06**	*	**14.35 ± 1.52**	**N↑***	**1.68 ± 0.17**	↑*	**135.92 ± 42.59**	**N***
		ZOL	1.02 ± 0.08		**12.87 ± 0.96**	↑	**1.56 ± 0.10**	↑	**170.35 ± 43.41**	**N**

Table 4. Tibial dynamic histomorphometry. "↑" or "↓" refers to a significant increase or decrease compared to week 2. "N", "O", or "A" refers to a significant difference compared to the NOM group, the OVX group, or all the other groups. Bonferroni correction was applied for the *p*-value calculation in the *post hoc* tests and multiple comparisons, after which the statistical significance level (alpha) was set to 0.05. The cells of statistical significance are in bold.

Time	Group	BMD (g/cm^3)		Tb.BV (mm^3)		Tb.BS (mm^2)		Tb.BV/TV (1)	
Week 2	NOM	**0.44 ± 0.05**	**A**	9.26 ± 1.13		555.12 ± 75.28		**45.15% ± 8.83%**	**A**
	OVX	**0.28 ± 0.04**	**A**	**5.16 ± 1.44**	**N**	460.73 ± 122.69		**21.95% ± 5.59%**	**A**
	ZOL	**0.38 ± 0.03**	**A**	**8.24 ± 1.23**	**O**	**630.64 ± 124.22**	**O**	**35.11% ± 4.88%**	**A**
Week 12	NOM	**0.47 ± 0.05**	**A**	**10.15 ± 1.21**	**A**	**548.31 ± 76.30**	**A**	**49.83% ± 6.65%**	**A**
	OVX	**0.22 ± 0.03**	**A↓**	**3.26 ± 0.68**	**A↓**	**233.60 ± 57.50**	**A↓**	**17.71% ± 2.48%**	**A**
	ZOL	**0.66 ± 0.06**	**A↑**	**22.57 ± 5.77**	**A↑**	**704.38 ± 109.81**	**A**	**73.09% ± 7.74%**	**A↑**
Time	**Group**	**Tb.Th (μm)**		**Tb.N (1/mm)**		**Tb.Sp (μm)**		**Conn.Dn (1/mm^3)**	
Week 2	NOM	**67.73 ± 7.42**	**A**	6.63 ± 0.79		88.52 ± 9.68		2579.78 ± 350.05	
	OVX	**49.37 ± 6.04**	**A**	**4.46 ± 1.08**	**N**	**131.10 ± 30.91**	**N**	1700.91 ± 579.30	
	ZOL	**55.82 ± 5.56**	**A**	**6.29 ± 0.88**	**O**	**94.82 ± 11.31**	**O**	**2661.36 ± 648.74**	**O**
Week 12	NOM	73.27 ± 7.14		**6.80 ± 0.58**	**A**	**84.80 ± 6.56**	**A**	2607.99 ± 421.45	
	OVX	**72.14 ± 6.68**	**↑**	**2.48 ± 0.49**	**A↓**	**153.97 ± 14.28**	**A**	**949.94 ± 297.08**	**A↓**
	ZOL	**89.96 ± 10.59**	**NO↑**	**8.17 ± 0.75**	**A↑**	**67.95 ± 8.46**	**A↓**	2482.04 ± 738.30	

3.4.1 Effects of treatment time

From week 2 to week 12: the ulnae of all the treatments showed increased Ct.BV and Ct.Ar (↑); the OVX tibiae showed decreased BMD, Tb.BV, Tb.BS, Tb.N, Conn.Dn (↓) and increased Tb.Th (↑); the ZOL tibiae showed increased BMD, Tb.BV, Tb.BV/TV, Tb.Th, Tb.N (↑) and decreased Tb.Sp (↓); The NOM tibiae did not show any change in time for these trabecular parameters.

3.4.2 Effects of treatment groups

Compared to the NOM group on week 2 (N): the OVX ulnae had lower TMD and Ct.Th; the ZOL ulnae had lower Ct.Th; the OVX and ZOL tibiae showed lower BMD, Tb.BV/TV, and Tb.Th.

Compared to the NOM group on week 12 (N): both OVX and ZOL ulnae showed lower Ct.Th; the ZOL ulnae (control) also showed higher Ct.BV and Ct.Ar; the OVX tibiae had higher Tb.Sp and lower BMD, Tb.BV, Tb.BS, Tb.BV/TV, Tb.N, Conn.Dn; the ZOL tibiae had higher BMD, Tb.BV, Tb.BS, Tb.BV/TV, Tb.Th, Tb.N, and lower Tb.Sp.

3.4.3 Effects of loading

On week 12, only the NOM and OVX group showed differences between their control and loaded ulnae (*): the NOM (loaded) had higher Ct.BV, Ct.Ar, and Ct.Th than the NOM (control); the OVX (loaded) had lower TMD, Ct.Th, and higher Ct.BV, Ct.Ar than the OVX (control).

3.5 Correlation analysis

The correlation results between SV/BV and the remodeling parameters are shown in Table 5. The formation remodeling parameters showed significant positive correlations with SV/BV, especially for MV/BV and MS/BS. The correlations were mostly negative for the resorption parameters, and the NOM rats had significant results for all the parameters. The correlation results between SV/BV and the mechanical properties are shown in Table 6. All the data points with statistical significance showed negative correlations.

Table 5. Spearman's rank-order correlation between SV/BV and the remodeling parameters. The Spearman's correlation coefficient was indicated if there was statistical significance ("**" for $p < 0.01$, "*" for $p < 0.05$, and "†" for $p < 0.15$). "/" refers to no statistical significance ($p > 0.15$).

	SV/BV - Ulna			SV/BV - Radius		
	NOM	OVX	ZOL	NOM	OVX	ZOL
MV/BV	0.86 **	0.87 **	0.77 **	0.41 †	0.55 *	0.61 *
MS/BS	0.82 **	0.85 **	0.75 **	0.40 †	0.50 *	0.57 *
MAR	0.87 **	0.89 **	0.54 *	/	/	/
EV/BV	-0.72 **	/	-0.48 †	-0.53 *	-0.47 †	/
ES/BS	-0.71 **	/	-0.48 †	-0.52 *	-0.49 †	/
MRR	-0.51 *	0.44 †	/	-0.39 †	/	/

Table 6. Spearman's rank-order correlation between SV/BV and the mechanical properties. The Spearman's correlation coefficient was indicated if there was statistical significance ("**" for $p < 0.01$, "*" for $p < 0.05$, and "†" for $p < 0.15$). "/" refers to no statistical significance ($p > 0.15$).

	SV/BV - Ulna			SV/BV - Radius		
	NOM	OVX	ZOL	NOM	OVX	ZOL
F_u	/	/	-0.26 †	-0.39 *	-0.39 *	-0.54 **
F_y	/	/	/	-0.33 †	-0.33 †	-0.63 **
S	/	/	/	-0.28 †	/	-0.59 **
D_{pre}	-0.34 †	/	/	/	/	/
U_{pre}	/	/	/	-0.31 †	/	-0.40 *
σ_u	-0.30 †	/	-0.31 †	-0.33 †	-0.45 **	/
σ_y	-0.32 †	/	-0.27 †	-0.32 †	-0.27 †	/
E	-0.39 *	/	/	/	/	-0.28 †
ϵ_{pre}	/	/	/	/	-0.30 †	/
u_{pre}	/	/	/	/	/	/

4 Discussion

4.1 The zoledronate treatment improves osteopenic conditions

The OVX rats had inferior bone qualities based on the results of microdamage accumulation (Fig. 4), bone material properties (Table 2), and histomorphometry (Table 3, Table 4). Ulna and radius did not have exactly the same tendencies on mechanical properties (Table 2, Supplementary Table 1), showing that the effects of ovariectomy are site-specific. Besides, ovariectomy-induced changes on cortical bone seemed to be less obvious than on trabecular bone (Table 3, Table 4, Supplementary Table 2). In fact, evidence from the literature suggests that bone loss in ovariectomized rats was quicker in trabecular bone than in cortical bone [35]. It is also easier to detect porosity in trabecular bone than in cortical bone using laboratory micro-CT scanners [85].

Nonetheless, the zoledronate treatment improved the osteopenic conditions of the ovariectomized rats in terms of reduced microdamage accumulation (Fig. 4), improved bone structural and material properties (Table 2, Supplementary Table 1), and enhanced microstructures (Table 3, Table 4). The beneficial effects of zoledronate treatment were significant for improving the bone strength (F_u, σ_u) without sacrificing the bone brittleness (D_{pre}, ϵ_{pre}) [86]. Past experimental studies showed that zoledronate treatment can improve the bending strength of long bones [66, 86], which was positively correlated with BMD [87]. Trabecular [87] and cortical [88] microstructure could also be improved by the zoledronate treatment. We confirm that zoledronate can improve the bone quality of ovariectomized rats in terms of bone microstructure and bending strength [42, 66, 89], which might be related to the increased TMD and BMD [52, 87].

4.2 The zoledronate treatment reduces cortical microdamage accumulation

The ZOL rats accumulated less microdamage than the other rats considering the following observations in Fig. 4: lower ΔSV/BV compared to the OVX radii and ulnae on day 15 post-loading; unchanged level of ΔSV/BV from day 5 to day 15 while the NOM and OVX had increased tendency in ulnae; lower ΔSV/BV compared to the NOM radii on day 5 post-loading. In comparison, the OVX rats had more microdamage despite lacking significant differences with the NOM rats, which might be due to the higher standard deviation of ΔSV/BV on day 15 post-loading

for the OVX. The NOM rats showed reduced damage level from day 5 to day 15 post-loading for the radius but the contrary was found for the ulna. In fact, the damage reduction observed in radius might be caused by remodeling-based damage repair [22, 90, 91] during the extra 10 days of recovery, while the increased damage level in ulna might be related to an excess amount of damage propagated relative to repair in the same time period [17, 92]. Moreover, the damage levels identified in ulna were higher than those of radius for all the rats according to the results of the t-test performed. Therefore, the initial amount of microdamage might be determinant for their state of repair and propagation.

Past studies with similar experimental designs on rat forelimb showed that the microdamage level SV/BV was the highest 5 days post-loading [24], and the damage density reduced after 2 weeks of recovery post-loading [23]. These findings are in line with the results of radius in the present study. However, we had contrasting results for ulna, where the NOM and OVX rats had increased SV/BV 15 days post-loading. These discrepancies might be caused by several differences in experimental design such as rats' gender and surgical treatments.

A previous study using an ovariectomized ovine model revealed that the zoledronate treatment increased the average crack density but reduced average crack length based on histology analysis [93]. A study using an osteolytic rat model showed reduced SV/BV level due to zoledronate treatment, evaluated by contrast-enhanced micro-CT [94]. As such, the reduced SV/BV level observed in the ZOL rats of the present study might have been caused by the reduced average length but not density, since the contrast enhanced micro-CT-based method is less sensitive than the histology-based method for damage detection. In general, the BPs treatment-related microdamage accumulation is more prominent in trabecular than in cortical bone [51].

Taken together, we conclude that the zoledronate treatment can reduce bone microdamage accumulation in cortical bone of osteoporotic rats. The balance between damage repair and propagation might be dependent on the initial damage quantity: damage repair could overcome propagation to reduce the damage level when the initial amount of damage is under a certain threshold (the case of the NOM radius); otherwise, damage propagation might exceed repair, leading to maintained or increased damage levels in the short term (the cases of the NOM and OVX ulna).

4.3 Microdamage accumulation correlates with periosteal bone formation

The correlation results in Table 5 showed that more microdamage accumulation is associated with increased bone formation and decreased bone resorption on the periosteum of ulna and radius. Based on visual observation in Fig. 3, the bone formed on the ulnar periosteum was mostly woven bone, which can help to restore the mechanical properties after tissue damage [95-97]. The bone formation parameters were less correlated to SV/BV for radius when compared to ulna, which might be explained by the relatively lower levels of ΔSV/BV in radii (section 3.1). Moreover, the results show that the correlation between the microdamage level and the woven bone formation is stronger for the OVX and NOM rats than the ZOL rats.

A past study with similar experimental design showed that zoledronate treatment led to higher periosteal bone formation compared to vehicle treatment [38]. Although ZOL rats in our study showed periosteal bone formation, this response was weaker and less correlated with microdamage accumulation compared to the NOM and OVX rats. The contrasting results might be caused by the different levels of loading intensity and zoledronate dosing frequency adopted. Nevertheless, we can confirm the cause and effect relationship between bone microdamage accumulation and periosteal bone formation [97], and the response of which was different between the normal, ovariectomized, and zoledronate-treated animals.

4.4 Limitations

In this study, the ovariectomy rat model was used to represent the post-menopausal osteoporosis in human. One of the disadvantages of rat models for microdamage studies is that rats do not have baseline intracortical remodeling due to the lack of Haversian systems [34-36]. This is different in the human body, which makes it harder to translate rodent-based research to clinical settings [98]. Rabbits show more advantages in this regard because they are considered to be the smallest laboratory animals with the capability of intracortical remodeling [27, 34, 99, 100]. Nonetheless, it is possible to initiate intracortical remodeling in rats with external stimulations such as mechanical loading [19]. The age of the rats is also an important factor for bone loss. The ovariectomy-induced bone loss is often considered osteopenic rather than osteoporosis at 3 months

old [34-36, 101], which is considered as a "mature rat model", in contrast to the "aged rat model" of 6 to 12 months old [33]. Besides the advantages of shorter experimental duration and greater availability from animal suppliers, the 3 months old rat model is also meaningful to investigate the microdamage accumulation in young adult populations who undergo rigorous physical training [102-104].

The analgesics used for the *in vivo* mechanical loading posed potential effects on bone metabolism. Although buprenorphine is usually considered a safe analgesic for laboratory animals [105], clinical findings suggest that it can reduce bone density by altering the osteoblastic activity [106]. Meloxicam (metacam), a type of nonsteroidal anti-inflammatory drug (NSAIDs), can potentially inhibit osteoblastic activities thus reduce bone formation [107-110]. Though we still observed significant periosteal bone formation in both ulna and radius post-loading, these responses might have been stronger without the use of meloxicam. Nonetheless, all the rats received the same analgesic dosage in the present study to ensure meaningful between-group comparisons. The adverse effects of the analgesics were assumed to be negligeable.

The present study leveraged the non-destructive nature of the *in vivo* micro-CT imaging to evaluate bone remodeling. However, rats' remodeling cycle is generally longer than the weekly scan interval [111-114]. Therefore, the remodeling parameters obtained were not representative of a complete formation or resorption cycle, but rather local averaged rates. Furthermore, the repeated anesthesia and immobilization associated with the *in vivo* imaging might have brought adverse effects to the animals' well-being [115-121]. There is no direct evidence that the repeated irradiation performed have caused significant bone loss to the scanned sites. Newer generations of micro-CT scanners might improve the image quality while reducing the scan duration, thus reducing the radiation doses. Deep learning algorithms also showed great potential for improving the interpretation of micro-CT scans [122].

In regard to the contrast-enhanced micro-CT imaging for microdamage evaluation, we used the same image resolution as for the *in vivo* scans but with higher voltage and current, longer exposure time, and more projections. This level of resolution was shown to be sufficient for detecting $BaSO_4$ stained microdamage in rodent long bones [25] and human samples [73]. Despite not being able to detect individual microdamages at this level of detail, the micro-CT-based SV/BV was proved to be well correlated with the histology-based damage parameters [24, 73]. Future studies can

leverage the power of deep learning algorithms for microdamage detection in micro-CT images [123, 124].

Lastly, the process of $BaSO_4$ staining might be able to alter the mechanical results. To account for this factor, we conducted a preliminary test with 6 pairs of contralateral forelimb samples, where the results showed that none of the mechanical properties were significantly different between the contralateral samples except for radial σ_u (about 11% lower for the stained samples). Therefore, we assumed that the between-group differences were not significantly changed by staining since all the samples went through the same processing steps. We considered that the advantages of reusing the same animals for mechanical testing outweighed their disadvantages based on the 3Rs principles [125].

5 Conclusion

In the present study, we developed and exploited an *in vivo* experimental platform combining the evaluation of bone microdamage, remodeling, mechanical properties as well as their correlations. Based on our results and literature evidence, we conclude that zoledronate treatment can reduce microdamage accumulation and improve the osteopenic conditions in cortical bone of ovariectomized rats. The balance between the damage repair and propagation might be dependent on the initial amount of damage. We confirm that the periosteal bone formation is correlated with the microdamage level, and the extent of which differs between normal, ovariectomized and zoledronate-treated animals. Our results provide insights to the clinical optimization of osteoporosis treatment using bisphosphonates. The same experimental concept can be applied in future studies on microdamage and drug testing.

Acknowledgements

This study was made possible by a micro-CT platform supported by the TransMedTech Institute. The authors would like to thank Dr Ryan K. Roeder, Dr Cari M. Whyne, Dr Da Jing, and their

teams for sharing the $BaSO_4$ staining procedure. Special thanks to Dr. Bettina Willie and her team for sharing the bone remodeling evaluation algorithm.

Funding

Funding was provided by the Natural Sciences and Engineering Research Council of Canada (NSERC/Discovery & NSERC/CREATE).

References

[1] D.B. Burr, R.B. Martin, M.B. Schaffler, E.L. Radin, Bone remodeling in response to in vivo fatigue microdamage, Journal of Biomechanics 18(3) (1985) 189-200.
[2] H.L. Frost, Presence of microscopic cracks in vivo in bone, Henry Ford Hospital Medical Journal 8(1) (1960) 25-35.
[3] T. Diab, D. Vashishth, Effects of damage morphology on cortical bone fragility, Bone 37(1) (2005) 96-102.
[4] T. Diab, K.W. Condon, D.B. Burr, D. Vashishth, Age-related change in the damage morphology of human cortical bone and its role in bone fragility, Bone 38(3) (2006) 427-431.
[5] D.B. Burr, C.H. Turner, P. Naick, M.R. Forwood, W. Ambrosius, M. Sayeed Hasan, R. Pidaparti, Does microdamage accumulation affect the mechanical properties of bone?, Journal of Biomechanics 31(4) (1998) 337-345.
[6] P. Zioupos, Accumulation of in-vivo fatigue microdamage and its relation to biomechanical properties in ageing human cortical bone, Journal of Microscopy 201(2) (2001) 270-278.
[7] C.A. Pattin, W.E. Caler, D.R. Carter, Cyclic mechanical property degradation during fatigue loading of cortical bone, Journal of Biomechanics 29(1) (1996) 69-79.
[8] D.R. Carter, W.E. Caler, D.M. Spengler, V.H. Frankel, Fatigue behavior of adult cortical bone: the influence of mean strain and strain range, Acta Orthopaedica Scandinavica 52(5) (1981) 481-490.
[9] T.E. Wenzel, M.B. Schaffler, D.P. Fyhrie, In vivo trabecular microcracks in human vertebral bone, Bone 19(2) (1996) 89-95.
[10] N.L. Fazzalari, M.R. Forwood, B.A. Manthey, K. Smith, P. Kolesik, Three-dimensional confocal images of microdamage in cancellous bone, Bone 23(4) (1998) 373-378.
[11] S. Nagaraja, T.L. Couse, R.E. Guldberg, Trabecular bone microdamage and microstructural stresses under uniaxial compression, Journal of Biomechanics 38(4) (2005) 707-716.
[12] P.J. Thurner, P. Wyss, R. Voide, M. Stauber, M. Stampanoni, U. Sennhauser, R. Müller, Time-lapsed investigation of three-dimensional failure and damage accumulation in trabecular bone using synchrotron light, Bone 39(2) (2006) 289-299.

[13] T. Diab, D. Vashishth, Morphology, localization and accumulation of in vivo microdamage in human cortical bone, Bone 40(3) (2007) 612-618.
[14] D. Vashishth, J. Koontz, S.J. Qiu, D. Lundin-Cannon, Y.N. Yeni, M.B. Schaffler, D.P. Fyhrie, In vivo diffuse damage in human vertebral trabecular bone, Bone 26(2) (2000) 147-152.
[15] D. Vashishth, K.E. Tanner, W. Bonfield, Experimental validation of a microcracking-based toughening mechanism for cortical bone, Journal of Biomechanics 36(1) (2003) 121-124.
[16] F.J. O'Brien, D. Taylor, T. Clive Lee, The effect of bone microstructure on the initiation and growth of microcracks, J. Orthop. Res. 23(2) (2005) 475-480.
[17] X. Wang, G.L. Niebur, Microdamage propagation in trabecular bone due to changes in loading mode, Journal of Biomechanics 39(5) (2006) 781-790.
[18] S. Mori, D.B. Burr, Increased intracortical remodeling following fatigue damage, Bone 14(2) (1993) 103-109.
[19] V. Bentolila, T.M. Boyce, D.P. Fyhrie, R. Drumb, T.M. Skerry, M.B. Schaffler, Intracortical remodeling in adult rat long bones after fatigue loading, Bone 23(3) (1998) 275-281.
[20] O. Verborgt, G.J. Gibson, M.B. Schaffler, Loss of osteocyte integrity in association with microdamage and bone remodeling after fatigue in vivo, Journal of Bone and Mineral Research 15(1) (2000) 60-67.
[21] D.B. Burr, Targeted and nontargeted remodeling, Bone 30(1) (2002) 2-4.
[22] Z. Seref-Ferlengez, J. Basta-Pljakic, O.D. Kennedy, C.J. Philemon, M.B. Schaffler, Structural and mechanical repair of diffuse damage in cortical bone in vivo, Journal of Bone and Mineral Research 29(12) (2014) 2537-2544.
[23] B.C. Herman, L. Cardoso, R.J. Majeska, K.J. Jepsen, M.B. Schaffler, Activation of bone remodeling after fatigue: Differential response to linear microcracks and diffuse damage, Bone 47(4) (2010) 766-772.
[24] X. Zhang, X. Liu, Z. Yan, J. Cai, F. Kang, S. Shan, P. Wang, M. Zhai, X. Edward Guo, E. Luo, D. Jing, Spatiotemporal characterization of microdamage accumulation in rat ulnae in response to uniaxial compressive fatigue loading, Bone 108 (2018) 156-164.
[25] T.L. Turnbull, J.A. Gargac, G.L. Niebur, R.K. Roeder, Detection of fatigue microdamage in whole rat femora using contrast-enhanced micro-computed tomography, Journal of Biomechanics 44(13) (2011) 2395-2400.
[26] J.A. Gargac, T.L. Turnbull, R.K. Roeder, G.L. Niebur, A probabilistic damage model based on direct 3-D correlation of strain to damage formation following fatigue loading of rat femora, Journal of the Mechanical Behavior of Biomedical Materials 30 (2014) 234-243.
[27] B.A. Coates, M.J. Silva, An animal trial to study damage and repair in ovariectomized rabbits, Journal of Biomechanics (2020) 109866.
[28] F.M. Lambers, A.R. Bouman, C.M. Rimnac, C.J. Hernandez, Microdamage caused by fatigue loading in human cancellous bone: relationship to reductions in bone biomechanical performance, PLoS One 8(12) (2013) e83662-e83662.
[29] c.d.p.o.o.p. NIH, diagnosis, therapy, Osteoporosis prevention, diagnosis, and therapy, JAMA 285(6) (2001) 785-795.
[30] H.P. Dimai, Use of dual-energy X-ray absorptiometry (DXA) for diagnosis and fracture risk assessment; WHO-criteria, T- and Z-score, and reference databases, Bone 104 (2017) 39-43.
[31] Y. Li, X. Xu, The role of estrogen in bone turnover with aging and age-related osteoporosis, Proceedings of the 2020 10th International Conference on Biomedical Engineering and Technology, Association for Computing Machinery, Tokyo, Japan, 2020, pp. 253–255.

[32] W.H.O. WHO, Assessment of fracture risk and its application to screening for postmenopausal osteoporosis: report of a WHO study group [meeting held in Rome from 22 to 25 June 1992], World Health Organization1994.
[33] D.N. Kalu, The ovariectomized rat model of postmenopausal bone loss, Bone and Mineral 15(3) (1991) 175-191.
[34] P.P. Lelovas, T.T. Xanthos, S.E. Thoma, G.P. Lyritis, I.A. Dontas, The laboratory rat as an animal model for osteoporosis research, Comparative medicine 58(5) (2008) 424-430.
[35] W. Jee, W. Yao, Overview: animal models of osteopenia and osteoporosis, J Musculoskelet Neuronal Interact 1(3) (2001) 193-207.
[36] U.T. Iwaniec, R.T. Turner, Chapter 39 - Animal models for osteoporosis, in: R. Marcus, D. Feldman, D.W. Dempster, M. Luckey, J.A. Cauley (Eds.), Osteoporosis (Fourth Edition), Academic Press, San Diego, 2013, pp. 939-961.
[37] U. Kettenberger, J. Ston, E. Thein, P. Procter, D.P. Pioletti, Does locally delivered zoledronate influence peri-implant bone formation? – Spatio-temporal monitoring of bone remodeling in vivo, Biomaterials 35(37) (2014) 9995-10006.
[38] A. Feher, A. Koivunemi, M. Koivunemi, R.K. Fuchs, D.B. Burr, R.J. Phipps, S. Reinwald, M.R. Allen, Bisphosphonates do not inhibit periosteal bone formation in estrogen deficient animals and allow enhanced bone modeling in response to mechanical loading, Bone 46(1) (2010) 203-207.
[39] Y. Hao, X. Wang, L. Wang, Y. Lu, Z. Mao, S. Ge, K. Dai, Zoledronic acid suppresses callus remodeling but enhances callus strength in an osteoporotic rat model of fracture healing, Bone 81 (2015) 702-711.
[40] X. Liu, X. Qu, T. Nie, Z. Zhai, H. Li, Z. Ouyang, A. Qin, S. Zhang, S. Zhang, Q. Fan, T. Tang, Z. Yu, M. Dai, The beneficial effects of bisphosphonate-enoxacin on cortical bone mass and strength in ovariectomized rats, Front Pharmacol 8(355) (2017).
[41] D.B. Burr, Bone biomechanics and bone quality: effects of pharmaceutical agents used to treat osteoporosis, Clinical Reviews in Bone and Mineral Metabolism 14(3) (2016) 197-217.
[42] J.A. Gasser, P. Ingold, A. Venturiere, V. Shen, J.R. Green, Long-term protective effects of zoledronic acid on cancellous and cortical bone in the ovariectomized rat, Journal of Bone and Mineral Research 23(4) (2008) 544-551.
[43] J. Åstrand, A.K. Harding, P. Aspenberg, M. Tägil, Systemic zoledronate treatment both prevents resorption of allograft bone and increases the retention of new formed bone during revascularization and remodelling. A bone chamber study in rats, BMC Musculoskeletal Disorders 7(1) (2006) 63.
[44] L.J. Kidd, N.R. Cowling, A.C.K. Wu, W.L. Kelly, M.R. Forwood, Bisphosphonate treatment delays stress fracture remodeling in the rat ulna, J. Orthop. Res. 29(12) (2011) 1827-1833.
[45] M.R. Allen, D.B. Burr, Mineralization, microdamage, and matrix: how bisphosphonates influence material properties of bone, IBMS BoneKEy 4 (2007) 49.
[46] R.D. Chapurlat, P.D. Delmas, Bone microdamage: a clinical perspective, Osteoporosis International 20(8) (2009) 1299-1308.
[47] J. Li, T. Mashiba, D.B. Burr, Bisphosphonate treatment suppresses not only stochastic remodeling but also the targeted repair of microdamage, Calcified Tissue International 69(5) (2001) 281-286.
[48] M.R. Allen, Recent advances in understanding bisphosphonate effects on bone mechanical properties, Current Osteoporosis Reports 16(2) (2018) 198-204.

[49] S. Ma, E.L. Goh, A. Jin, R. Bhattacharya, O.R. Boughton, B. Patel, A. Karunaratne, N.T. Vo, R. Atwood, J.P. Cobb, U. Hansen, R.L. Abel, Long-term effects of bisphosphonate therapy: perforations, microcracks and mechanical properties, Scientific Reports 7 (2017) 10.
[50] T. Mashiba, T. Hirano, C.H. Turner, M.R. Forwood, C.C. Johnston, D.B. Burr, Suppressed bone turnover by bisphosphonates increases microdamage accumulation and reduces some biomechanical properties in dog rib, Journal of Bone and Mineral Research 15(4) (2000) 613-620.
[51] M.R. Allen, D.B. Burr, Bisphosphonate effects on bone turnover, microdamage, and mechanical properties: What we think we know and what we know that we don't know, Bone 49(1) (2011) 56-65.
[52] D.B. Burr, Fifty years of bisphosphonates: What are their mechanical effects on bone?, Bone (2020) 115518.
[53] D.M. Black, B. Abrahamsen, M.L. Bouxsein, T. Einhorn, N. Napoli, Atypical femur fractures: review of epidemiology, relationship to bisphosphonates, prevention, and clinical management, Endocrine Reviews 40(2) (2018) 333-368.
[54] D.M. Black, K. Condra, R. Eastell, Bisphosphonates and the risk of atypical femur fractures, Bone (2021) 116297.
[55] L. Gedmintas, D.H. Solomon, S.C. Kim, Bisphosphonates and risk of subtrochanteric, femoral shaft, and atypical femur fracture: A systematic review and meta-analysis, Journal of Bone and Mineral Research 28(8) (2013) 1729-1737.
[56] E. Shane, D. Burr, B. Abrahamsen, R.A. Adler, T.D. Brown, A.M. Cheung, F. Cosman, J.R. Curtis, R. Dell, D.W. Dempster, P.R. Ebeling, T.A. Einhorn, H.K. Genant, P. Geusens, K. Klaushofer, J.M. Lane, F. McKiernan, R. McKinney, A. Ng, J. Nieves, R. O'Keefe, S. Papapoulos, T.S. Howe, M.C. van der Meulen, R.S. Weinstein, M.P. Whyte, Atypical subtrochanteric and diaphyseal femoral fractures: second report of a task force of the American Society for Bone and Mineral Research, Journal of Bone and Mineral Research 29(1) (2014) 1-23.
[57] S. Ohta, R. Ikeguchi, T. Noguchi, Y. Kaizawa, S. Matsuda, Intractable fractures of the bilateral proximal ulnae after 8 years of zoledronate treatment for breast cancer bone metastasis, The Journal of Hand Surgery 47(4) (2022) 393.e1-393.e7.
[58] S.H.S. Tan, S. Saseendar, B.H.M. Tan, A. Pawaskar, V.P. Kumar, Ulnar fractures with bisphosphonate therapy: a systematic review of published case reports, Osteoporosis International 26(2) (2015) 421-429.
[59] B.H. Oh, Y.M. Heo, J.W. Yi, T.G. Kim, J.S. Lee, Atypical fracture of the proximal shaft of the ulna associated with prolonged bisphosphonate therapy, cios 10(3) (2018) 389-392.
[60] J. Moon, N. Bither, T. Lee, Atypical forearm fractures associated with long-term use of bisphosphonate, Archives of Orthopaedic and Trauma Surgery 133(7) (2013) 889-892.
[61] E. Shane, S. Khosla, D. Burr, Chapter 81 - Osteonecrosis of the jaw and atypical femoral fractures, in: R. Marcus, D. Feldman, D.W. Dempster, M. Luckey, J.A. Cauley (Eds.), Osteoporosis (Fourth Edition), Academic Press, San Diego, 2013, pp. 1873-1908.
[62] S. Khosla, D. Burr, J. Cauley, D.W. Dempster, P.R. Ebeling, D. Felsenberg, R.F. Gagel, V. Gilsanz, T. Guise, S. Koka, L.K. McCauley, J. McGowan, M.D. McKee, S. Mohla, D.G. Pendrys, L.G. Raisz, S.L. Ruggiero, D.M. Shafer, L. Shum, S.L. Silverman, C.H. Van Poznak, N. Watts, S.-B. Woo, E. Shane, Bisphosphonate-associated osteonecrosis of the jaw: report of a task force of the American Society for Bone and Mineral Research, Journal of Bone and Mineral Research 22(10) (2007) 1479-1491.
[63] R.E. Marx, Pamidronate (Aredia) and zoledronate (Zometa) induced avascular necrosis of the jaws: a growing epidemic, J. Oral Maxillofac. Surg. 61(9) (2003) 1115-1117.

[64] J.Y. Wang, L. Huo, R.Q. Yu, N.J. Rao, W.W. Lu, L.W. Zheng, Skeletal site-specific response of jawbones and long bones to surgical interventions in rats treated with zoledronic acid, BioMed Research International 2019 (2019) 5138175.
[65] L.E. Mulcahy, C.M. Curtin, R.J. McCoy, F.J. O'Brien, D. Taylor, T.C. Lee, G.P. Duffy, The effect of bisphosphonate treatment on the biochemical and cellular events during bone remodelling in response to microinjury stimulation, Eur Cell Mater 30 (2015) 271-81.
[66] M.W. Aref, E.M.B. McNerny, D. Brown, K.J. Jepsen, M.R. Allen, Zoledronate treatment has different effects in mouse strains with contrasting baseline bone mechanical phenotypes, Osteoporosis International 27(12) (2016) 3637-3643.
[67] A.G. Robling, F.M. Hinant, D.B. Burr, C.H. Turner, Improved Bone Structure and Strength After Long-Term Mechanical Loading Is Greatest if Loading Is Separated Into Short Bouts, Journal of Bone and Mineral Research 17(8) (2002) 1545-1554.
[68] T. Mustafy, A. Benoit, I. Londono, F. Moldovan, I. Villemure, Can repeated in vivo micro-CT irradiation during adolescence alter bone microstructure, histomorphometry and longitudinal growth in a rodent model?, PLoS One 13(11) (2018) e0207323.
[69] H.J. Johnson, M.M. McCormick, L. Ibanez, The ITK software guide book 2: design and functionality, Kitware, Inc.2015.
[70] A.I. Birkhold, H. Razi, G.N. Duda, R. Weinkamer, S. Checa, B.M. Willie, Mineralizing surface is the main target of mechanical stimulation independent of age: 3D dynamic in vivo morphometry, Bone 66 (2014) 15-25.
[71] M.L. Bouxsein, S.K. Boyd, B.A. Christiansen, R.E. Guldberg, K.J. Jepsen, R. Müller, Guidelines for assessment of bone microstructure in rodents using micro–computed tomography, Journal of Bone and Mineral Research 25(7) (2010) 1468-1486.
[72] A.I. Birkhold, H. Razi, G.N. Duda, R. Weinkamer, S. Checa, B.M. Willie, The periosteal bone surface is less mechano-responsive than the endocortical, Scientific Reports 6(1) (2016) 23480.
[73] M.D. Landrigan, J. Li, T.L. Turnbull, D.B. Burr, G.L. Niebur, R.K. Roeder, Contrast-enhanced micro-computed tomography of fatigue microdamage accumulation in human cortical bone, Bone 48(3) (2011) 443-450.
[74] H. Leng, X. Wang, R.D. Ross, G.L. Niebur, R.K. Roeder, Micro-computed tomography of fatigue microdamage in cortical bone using a barium sulfate contrast agent, Journal of the Mechanical Behavior of Biomedical Materials 1(1) (2008) 68-75.
[75] C. Choudhari, K. Chan, M.K. Akens, C.M. Whyne, μFE models can represent microdamaged regions of healthy and metastatically involved whole vertebrae identified through histology and contrast enhanced μCT imaging, Journal of Biomechanics 49(7) (2016) 1103-1110.
[76] J.L. Schriefer, A.G. Robling, S.J. Warden, A.J. Fournier, J.J. Mason, C.H. Turner, A comparison of mechanical properties derived from multiple skeletal sites in mice, Journal of Biomechanics 38(3) (2005) 467-475.
[77] J.M. Wallace, Chapter 7 - Skeletal hard tissue biomechanics, in: D.B. Burr, M.R. Allen (Eds.), Basic and Applied Bone Biology (Second Edition), Academic Press2019, pp. 125-140.
[78] D.B. Burr, Z. Liu, M.R. Allen, Duration-dependent effects of clinically relevant oral alendronate doses on cortical bone toughness in beagle dogs, Bone 71 (2015) 58-62.
[79] R. Domander, A. Felder, M. Doube, BoneJ2 - refactoring established research software [version 2; peer review: 3 approved], Wellcome Open Research 6(37) (2021).
[80] J. Schindelin, I. Arganda-Carreras, E. Frise, V. Kaynig, M. Longair, T. Pietzsch, S. Preibisch, C. Rueden, S. Saalfeld, B. Schmid, J.-Y. Tinevez, D.J. White, V. Hartenstein, K. Eliceiri, P.

Tomancak, A. Cardona, Fiji: an open-source platform for biological-image analysis, Nature Methods 9(7) (2012) 676-682.
[81] J. Jaccard, Interaction effects in factorial analysis of variance, Thousand Oaks, California, 1998.
[82] Laerd Statistics, Three-way mixed ANOVA (with one between-subjects and two within-subjects factors) using SPSS Statistics. Statistical tutorials and software guides, 2015. https://statistics.laerd.com/premium/spss/mabww/mabww-in-spss.php.
[83] D.G. Altman, Practical statistics for medical research, Chapman and Hall, London and New York, 1991.
[84] G. Keppel, Design and analysis : a researcher's handbook, 4th ed. ed., Pearson Prentice Hall, Upper Saddle River, N.J. :, 2004.
[85] D. Cooper, A. Turinsky, C. Sensen, B. Hallgrimsson, Effect of voxel size on 3D Micro-CT analysis of cortical bone porosity, Calcified Tissue International 80(3) (2007) 211-219.
[86] L.E. Bilston, D.G. Little, N.C. Smith, P. Williams, J. Briody, Zoledronic acid improves the mechanical properties of normal and healing bone, Clinical Biomechanics 17(9) (2002) 716-718.
[87] S.B. Hornby, G.P. Evans, S.L. Hornby, A. Pataki, M. Glatt, J.R. Green, Long-term zoledronic acid treatment increases bone structure and mechanical strength of long bones of ovariectomized adult rats, Calcified Tissue International 72(4) (2003) 519-527.
[88] V.A. Stadelmann, N. Bonnet, D.P. Pioletti, Combined effects of zoledronate and mechanical stimulation on bone adaptation in an axially loaded mouse tibia, Clinical Biomechanics 26(1) (2011) 101-105.
[89] C.N. Meixner, M.W. Aref, A. Gupta, E.M.B. McNerny, D. Brown, J.M. Wallace, M.R. Allen, Raloxifene improves bone mechanical properties in mice previously treated with zoledronate, Calcified Tissue International 101(1) (2017) 75-81.
[90] Z. Seref-Ferlengez, O.D. Kennedy, M.B. Schaffler, Bone microdamage, remodeling and bone fragility: how much damage is too much damage?, Bonekey Rep 4 (2015) 644-644.
[91] D.B. Burr, Repair mechanisms for microdamage in bone, Journal of Bone and Mineral Research 29(12) (2014) 2534-2536.
[92] Z. Wu, A.J. LaNeve, G.L. Niebur, In vivo microdamage is an indicator of susceptibility to initiation and propagation of microdamage in human femoral trabecular bone, Bone 55(1) (2013) 208-215.
[93] O. Brennan, O.D. Kennedy, T.C. Lee, S.M. Rackard, F.J. O'Brien, Effects of estrogen deficiency and bisphosphonate therapy on osteocyte viability and microdamage accumulation in an ovine model of osteoporosis, J. Orthop. Res. 29(3) (2011) 419-424.
[94] A. Tolgyesi, C. Huang, M. Akens, M. Hardisty, C. Whyne, Treatment effects on microdamage accumulation and load to failure in osteolytic rat vertebrae, Orthopaedic Proceedings 104-B(SUPP_12) (2022) 11-11.
[95] B.A. Uthgenannt, M.J. Silva, Use of the rat forelimb compression model to create discrete levels of bone damage in vivo, Journal of Biomechanics 40(2) (2007) 317-324.
[96] G.R. Wohl, D.A. Towler, M.J. Silva, Stress fracture healing: Fatigue loading of the rat ulna induces upregulation in expression of osteogenic and angiogenic genes that mimic the intramembranous portion of fracture repair, Bone 44(2) (2009) 320-330.
[97] B.A. Uthgenannt, M.H. Kramer, J.A. Hwu, B. Wopenka, M.J. Silva, Skeletal self-repair : stress fracture healing by rapid formation and densification of woven bone, Journal of Bone and Mineral Research 22(10) (2007) 1548-1556.

[98] M.R. Allen, Preclinical models for skeletal research: how commonly used species mimic (or don't) aspects of human bone, Toxicol. Pathol. 45(7) (2017) 851-854.
[99] E.G. Buettmann, M.J. Silva, Development of an in vivo bone fatigue damage model using axial compression of the rabbit forelimb, Journal of Biomechanics 49(14) (2016) 3564-3569.
[100] A.S. Turner, Animal models of osteoporosis—necessity and limitations, Eur Cell Mater 1(66-81) (2001) 13.
[101] D.B. Kimmel, E.L. Moran, E.R. Bogoch, Animal models of osteopenia or osteoporosis, Animal models in orthopaedic research, CRC Press2020, pp. 279-305.
[102] N. Hod, G. Fire, I. Cohen, Stress fracture of the ulna in a military recruit, Israel Medical Association Journal (2006).
[103] K. Bigosinski, T. Palmer, K. Weber, J. Evola, Ulnar shaft stress fracture in a high school softball pitcher, Sports Health 2(2) (2010) 116-118.
[104] W.W. Cole, M.K. Mulcahey, F.H. Savoie, Upper extremity stress fractures, in: T.L. Miller, C.C. Kaeding (Eds.), Stress fractures in athletes: diagnosis and management, Springer International Publishing, Cham, 2020, pp. 181-189.
[105] M. Guarnieri, C. Brayton, L. DeTolla, N. Forbes-McBean, R. Sarabia-Estrada, P. Zadnik, Safety and efficacy of buprenorphine for analgesia in laboratory mice and rats, Lab Anim (NY) 41(11) (2012) 337-343.
[106] F. Coluzzi, J. Pergolizzi, R.B. Raffa, C. Mattia, The unsolved case of "bone-impairing analgesics": the endocrine effects of opioids on bone metabolism, Therap. Clin. Risk Manag. 11 (2015) 515-523.
[107] I. Pountos, T. Georgouli, G.M. Calori, P.V. Giannoudis, Do nonsteroidal anti-inflammatory drugs affect bone healing? A critical analysis, ScientificWorldJournal 2012 (2012) 606404.
[108] J. Cottrell, J.P. O'Connor, Effect of non-steroidal anti-inflammatory drugs on bone healing, Pharmaceuticals (Basel) 3(5) (2010) 1668-1693.
[109] J.-K. Chang, G.-J. Wang, S.-T. Tsai, M.-L. Ho, Nonsteroidal anti-inflammatory drug effects on osteoblastic cell cycle, cytotoxicity, and cell death, Connective Tissue Research 46(4-5) (2005) 200-210.
[110] M.A. Burch, A. Keshishian, C. Wittmann, D. Nehrbass, U. Styger, G. Muthukrishnan, D. Arens, V.A. Stadelmann, R.G. Richards, T.F. Moriarty, K. Thompson, The non-steroidal anti-inflammatory drug carprofen negatively impacts new bone formation and antibiotic efficacy in a rat model of orthopaedic-device-related infection, Eur Cell Mater 41 (2021) 739-755.
[111] R. Baron, R. Tross, A. Vignery, Evidence of sequential remodeling in rat trabecular bone: Morphology, dynamic histomorphometry, and changes during skeletal maturation, The Anatomical Record 208(1) (1984) 137-145.
[112] R.S. Weinstein, R.L. Jilka, A.M. Parfitt, S.C. Manolagas, Inhibition of osteoblastogenesis and promotion of apoptosis of osteoblasts and osteocytes by glucocorticoids. Potential mechanisms of their deleterious effects on bone, The Journal of Clinical Investigation 102(2) (1998) 274-82.
[113] R.L. Jilka, The relevance of mouse models for investigating age-related bone loss in humans, The Journals of Gerontology: Series A 68(10) (2013) 1209-17.
[114] P.T. Van, A. Vignery, R. Baron, Cellular kinetics of the bone remodeling sequence in the rat, The Anatomical Record 202(4) (1982) 445-451.
[115] K. Hohlbaum, B. Bert, S. Dietze, R. Palme, H. Fink, C. Thöne-Reineke, Severity classification of repeated isoflurane anesthesia in C57BL/6JRj mice—Assessing the degree of distress, PLoS One 12(6) (2017) e0179588.

[116] C.E. Hotchkiss, R. Brommage, M. Du, C.P. Jerome, The anesthetic isoflurane decreases ionized calcium and increases parathyroid hormone and osteocalcin in cynomolgus monkeys, Bone 23(5) (1998) 479-484.
[117] B. Kádár, K. Gombos, E. Szele, A. Beregi, Z. Varga, A. Sebestyén, I. Ember, Effects of isoflurane exposure on oncogene and tumour suppressor gene expressions in vital organs of cba/ca mice, In Vivo 21(5) (2007) 861-865.
[118] H. Kim, E. Oh, H. Im, J. Mun, M. Yang, J.-Y. Khim, E. Lee, S.H. Lim, M.H. Kong, M. Lee, D. Sul, Oxidative damages in the DNA, lipids, and proteins of rats exposed to isofluranes and alcohols, Toxicology 220(2) (2006) 169-178.
[119] P. Patterson-Buckendahl, M. Rusnák, K. Fukuhara, R. Kvetnaňský, Repeated immobilization stress reduces rat vertebral bone growth and osteocalcin, American Journal of Physiology-Regulatory, Integrative and Comparative Physiology 280(1) (2001) R79-R86.
[120] W.C. Stevens, E.I. Eger, A. White, M.J. Halsey, W. Munger, R.D. Gibbons, W. Dolan, R. Shargel, Comparative toxicities of halothane, isoflurane, and diethyl ether at subanesthetic concentrations in laboratory animals, The Journal of the American Society of Anesthesiologists 42(4) (1975) 408-418.
[121] L.M. Stollings, L.-J. Jia, P. Tang, H. Dou, B. Lu, Y. Xu, Immune modulation by volatile anesthetics, Anesthesiology 125(2) (2016) 399-411.
[122] Y.D. Wang, R.T. Armstrong, P. Mostaghimi, Boosting resolution and recovering texture of 2D and 3D micro-CT images with deep learning, Water Resources Research 56(1) (2020) e2019WR026052.
[123] R. Caron, I. Londono, L. Seoud, I. Villemure, Segmentation of trabecular bone microdamage in Xray microCT images using a two-step deep learning method, Journal of the Mechanical Behavior of Biomedical Materials 137 (2023) 105540.
[124] F. Buccino, I. Aiazzi, A. Casto, B. Liu, M.C. Sbarra, G. Ziarelli, G. Banfi, L.M. Vergani, The synergy of synchrotron imaging and convolutional neural networks towards the detection of human micro-scale bone architecture and damage, Journal of the Mechanical Behavior of Biomedical Materials 137 (2023) 105576.
[125] L.U. Sneddon, L.G. Halsey, N.R. Bury, Considering aspects of the 3Rs principles within experimental animal biology, Journal of Experimental Biology 220(17) (2017) 3007-3016.